

Magnetization-direction tunable nodal-line and Weyl phases

Zeying Zhang,^{1,2} Qiang Gao,² Cheng-Cheng Liu,¹ Hongbin Zhang,^{2,*} and Yugui Yao^{1,†}
¹Beijing Key Laboratory of Nanophotonics and Ultrafine Optoelectronic Systems, School of Physics,
 Beijing Institute of Technology, Beijing 100081, China
²Institute of Materials Science, TU Darmstadt, 64287 Darmstadt, Germany



(Received 8 June 2018; published 7 September 2018)

We propose a spinless symmetry-based three-band tight-binding model with the coexistence of nodal-line and Weyl points, after considering spin-orbital coupling and different magnetization directions. It is confirmed that the number of Weyl points and nodal lines can be tuned by the magnetization direction. The combination of time-reversal symmetry and mirror reflection symmetry plays a crucial role in protecting the degeneracy of nodal lines. Moreover, we put forward a different class of materials C_4CrX_3 ($X = \text{Ge}$ and Si) which host such a nontrivial semimetallic phase.

DOI: [10.1103/PhysRevB.98.121103](https://doi.org/10.1103/PhysRevB.98.121103)

Being topological materials with vanishing band gaps, Weyl semimetals [1] and nodal-line semimetals [2] have been intensively studied both theoretically [1–14] and experimentally [15–20]. In general, for compounds with a nontrivial topological nature, symmetry plays a crucial role, which constrains the Hamiltonian and leads to so-called symmetry protected topological orders [21]. The band dispersion of the Weyl points and nodal lines in momentum space has a twofold degeneracy, leading to nontrivial surface states, which are Fermi arc [4] and drumhead states [22,23], respectively. Nevertheless, as the quantum anomalous Hall insulators, no particular symmetry is required for the occurrence of Weyl points, where the breaking of either time-reversal symmetry (TRS) or spatial inversion symmetry is in favor of giving rise to Weyl points [11]. On the other hand, the occurrence of a nodal line requires more symmetries than that of Weyl points because the codimension of a nodal line is less than the Weyl points [2]. In particular, magnetic topological semimetals are very interesting [24–27], including both ferromagnets [20,28–32] and antiferromagnetic materials [33–35]. From an application point of view, nontrivial topological states in magnetic materials are of particular interest. The minimal number (two) of Weyl fermions makes it easier to observe negative longitudinal magnetoresistance [31,36], and also to engineer quantum anomalous Hall thin films. It is noted that the nontrivial topological electronic states are entangled fundamentally with the magnetic degrees of freedom, leading to tunable properties such as spin-orbit torque [34,37,38].

In this Rapid Communication, we investigate a lattice model allowing for the coexistence of Weyl points and nodal lines which can be further tailored by the magnetization direction, and propose a possible realization in a class of materials. Based on a symmetry analysis using a three-band tight-binding lattice model, it is demonstrated that the number of Weyl points and nodal lines can be manipulated by varying

the magnetization direction via spin-orbit coupling (SOC). It is further shown that such a model can be realized in C_4CrX_3 ($X = \text{Si}$ and Ge) by explicit density functional theory (DFT) calculations, where the topological properties are investigated in detail. We expect that such an effective tailoring can be realized in other magnetic materials with the same point group, requiring further experimental and theoretical investigations.

We start with a simple lattice model with a D_{2d} point group symmetry (Fig. 1). There are two mirror reflection planes, namely, the (110) and (1 $\bar{1}$ 0) planes, and three C_2 rotation axes parallel to the x , y , z axis, as shown in Fig. 1. It is supposed that the bands around the Fermi energy (E_F) originate from the d orbitals of the A atoms located at the corners. From the character table of the D_{2d} point group, there are three one-dimensional irreducible representations and one two-dimensional irreducible representation. For simplicity, we use three d orbitals, d_{z^2} , $d_{x^2-y^2}$, and d_{xy} , as our basis, corresponding to three one-dimensional irreducible representations. Neglecting SOC first and considering only the nearest-neighbor and next-nearest-neighbor hoppings, in the basis of $|\varphi_i\rangle = \{|d_{z^2}\rangle, |d_{x^2-y^2}\rangle, |d_{xy}\rangle\}$, the Hamiltonian can be expressed as

$$H_{ij}(\mathbf{k}) = \sum_{\mathbf{R}} e^{i\mathbf{k}\cdot\mathbf{R}} t_{ij}(\mathbf{R}),$$

$$t_{ij}(\mathbf{R}) = \langle \varphi_i(\mathbf{R}) | H | \varphi_j(\mathbf{r} - \mathbf{R}) \rangle, \quad (1)$$

where t_{ij} denotes the hopping integrals for neighboring sites with displacement \mathbf{R} which are obtained following Ref. [39],

$$t_{ij}(\mathbf{R}\mathbf{R}_n) = D_i(\mathbf{R})t_{ij}(\mathbf{R}_n)[D_j(\mathbf{R})]^\dagger, \quad (2)$$

with $D_i(\mathbf{R})$ the matrix of the i th irreducible representations. The corresponding Hamiltonian matrix elements can be explicitly written as

$$H_{\text{diag}} = \epsilon + \alpha(\cos k_x + \cos k_y) + \beta \cos k_z + \gamma \cos k_x \cos(k_y)$$

$$+ \delta(\cos k_x \cos k_z + \cos k_y \cos k_z),$$

$$H_{12} = \alpha(\cos k_x - \cos k_y) + \delta(\cos k_x \cos k_z - \cos k_y \cos k_z),$$

*hzhang@tmm.tu-darmstadt.de

†ygyao@bit.edu.cn

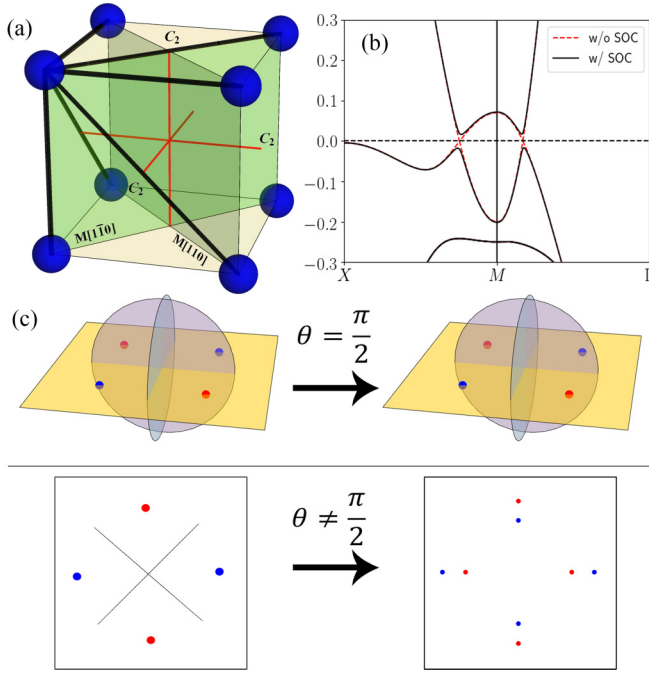


FIG. 1. (a) Sketch of the lattice model. The blue spheres are eight equivalence A atoms forming a simple cubic structure, the red lines denote three C_2 rotation axes, and green planes represent two mirror planes. (b) Band structure with and without SOC. (c) Schematic plot of the evolution of the Weyl points and nodal lines with different magnetization directions θ . The blue (red) points denote Weyl nodes whose chirality is $+1$ (-1); notice that when $\theta \neq \frac{\pi}{2}$ (top view of the three-dimensional plot), the Weyl points are no longer on the high symmetry lines.

$$\begin{aligned}
 H_{13} &= i\beta \sin k_z + \gamma \sin k_x \sin(k_y) \\
 &\quad + i\delta(\cos k_x \sin k_z + \cos k_y \sin k_z), \\
 H_{23} &= i\delta(\cos k_x \sin k_z - \cos k_y \sin k_z), \\
 H_{ij} &= H_{ji}^*.
 \end{aligned} \tag{3}$$

H_{ij} is the function of ϵ , α , β , γ , and δ which denotes the hopping integrals t_{ij} tabulated in the Supplemental Material [40], and k_i ($i = x, y, z$) are the Cartesian components of the \mathbf{k} vector in the Brillouin zone. It is noted that the hopping integrals for Fig. 1(b) are obtained by fitting the DFT band structure of $C_4\text{CrSi}_3$. It is easy to find out that when $k_x = k_y$ or $k_x = -k_y$, i.e., \mathbf{k} vectors on the mirror plane, the Hamiltonian becomes block-diagonal. This is also true when $(k_x = \pi, k_z = 0)$ or $(k_y = \pi, k_z = 0)$, i.e., \mathbf{k} vectors on the C_2 rotation axes. In such cases, it is observed that there exist nodal lines and Weyl points in the corresponding planes and lines, which will be discussed in detail.

Generally, combined with the TRS breaking, SOC will lower symmetry further and hence can lift the degeneracy in the electronic structure. In this case, specific symmetries are required to protect the Weyl points and nodal lines. For instance, Niu *et al.* have shown that mirror symmetry is crucial for the existence of nodal lines in two-dimensional magnetic systems [41]. In our three-dimensional model, this is also true, i.e., the nodal line exists in the presence of SOC. More interestingly, it is observed that the magnetization direction

can be used to tailor the topological properties. For a general spin quantization direction \mathbf{m} characterized by (θ, ϕ) where θ (ϕ) denotes the polar (azimuthal) angle, the “spin-up” and “spin-down” spinor can be written as

$$\begin{aligned}
 |\uparrow\rangle_{\mathbf{m}} &= e^{-i\frac{\phi}{2}} \cos \frac{\theta}{2} |\uparrow\rangle + e^{i\frac{\phi}{2}} \sin \frac{\theta}{2} |\downarrow\rangle, \\
 |\downarrow\rangle_{\mathbf{m}} &= -e^{-i\frac{\phi}{2}} \sin \frac{\theta}{2} |\uparrow\rangle + e^{i\frac{\phi}{2}} \cos \frac{\theta}{2} |\downarrow\rangle,
 \end{aligned} \tag{4}$$

where $0 \leq \theta \leq \pi$, $0 \leq \phi < 2\pi$, and $|\uparrow\rangle$ and $|\downarrow\rangle$ are the eigenvectors of \hat{s}_z . The SOC term corresponding to a general magnetization direction \mathbf{m} in the basis of our lattice model is [42]

$$H_{\text{SOC}} = \frac{1}{2} i\xi \begin{bmatrix} 0 & 0 & 0 & 0 & 0 & 0 \\ 0 & 0 & \cos \theta & 0 & 0 & -\sin \theta \\ 0 & -\cos \theta & 0 & 0 & \sin \theta & 0 \\ 0 & 0 & 0 & 0 & 0 & 0 \\ 0 & 0 & -\sin \theta & 0 & 0 & -\cos \theta \\ 0 & \sin \theta & 0 & 0 & \cos \theta & 0 \end{bmatrix}. \tag{5}$$

We note that H_{SOC} is only a function of polar angle θ . That is, the band degeneracy and thus the topological properties are directly coupled to the magnetization direction \mathbf{m} . From the symmetry point of view, all the relevant operations can be obtained by

$$P_R^{-1} H(\mathbf{k}) P_R = H(R^{-1}\mathbf{k}), \tag{6}$$

where P_R (e.g., mirror operator M or C_2 rotation operator P_C) is the symmetry operator of R , and R is the 3×3 matrix defining the three-dimensional symmetry operation. Moreover, eigenvalues for the mirror operator of $|d_{xy}\rangle$ and $|d_{x^2-y^2}\rangle$ are ± 1 . Considering the spin degree of freedom, we can obtain the matrix representations of the symmetry operator with SOC,

$$P_{\text{SOC}} = (\boldsymbol{\sigma} \cdot \mathbf{a}) \otimes P, \tag{7}$$

where $\boldsymbol{\sigma} = (\sigma_0, \sigma_1, \sigma_2, \sigma_3)$ are the identity matrix and Pauli matrices, \mathbf{a} is the coefficient of the Pauli matrix, and P is the symmetry operator without SOC. Taking the (110) mirror plane as an example, as magnetization is a pseudovector, i.e., the magnetization direction changes (is invariant) when it is parallel (perpendicular) to the mirror plane, $\mathbf{i} \rightarrow -\mathbf{j}$, $\mathbf{j} \rightarrow -\mathbf{i}$, $\mathbf{k} \rightarrow -\mathbf{k}$, the magnetization direction $\mathbf{m} = \cos \phi \sin \theta \mathbf{i} + \sin \phi \sin \theta \mathbf{j} + \cos \theta \mathbf{k}$ will change to $\mathbf{m}_M = \cos(\frac{\pi}{2} - \phi) \sin(\theta + \pi) \mathbf{i} + \sin(\frac{\pi}{2} - \phi) \sin(\theta + \pi) \mathbf{j} + \cos(\theta + \pi) \mathbf{k}$, hence $\phi \rightarrow (\frac{\pi}{2} - \phi)$, $\theta \rightarrow (\theta + \pi)$. Therefore, it is easy to get $\boldsymbol{\sigma} \cdot \mathbf{a}$ by $|\phi, \theta\rangle = \boldsymbol{\sigma} \cdot \mathbf{a} |\frac{\pi}{2} - \phi, \theta + \pi\rangle$, correspondingly $\boldsymbol{\sigma} \cdot \mathbf{a} = \frac{i}{\sqrt{2}}(\sigma_x - \sigma_y)$. For the (1 $\bar{1}$ 0) mirror plane, it is easy to show that $\boldsymbol{\sigma} \cdot \mathbf{a} = \frac{i}{\sqrt{2}}(\sigma_x + \sigma_y)$. In the same spirit, for $C_{2(z)}$ ($C_{2(x)}$, and $C_{2(y)}$), $\boldsymbol{\sigma} \cdot \mathbf{a} = i\sigma_z$ ($i\sigma_x$, and $i\sigma_y$), respectively.

Using the spin matrices for all the relevant symmetry operations obtained so far, it is straightforward to find out the change in the electronic structure induced by H_{SOC} . When the spin matrices for the mirror and C_2 symmetries can be expressed as $\boldsymbol{\sigma} \cdot \mathbf{a} = \alpha\sigma_y + \beta\sigma_z$, where α and β are arbitrary complex constants, $[H, M] = 0$, $[H, P_C] = 0$, if and only if

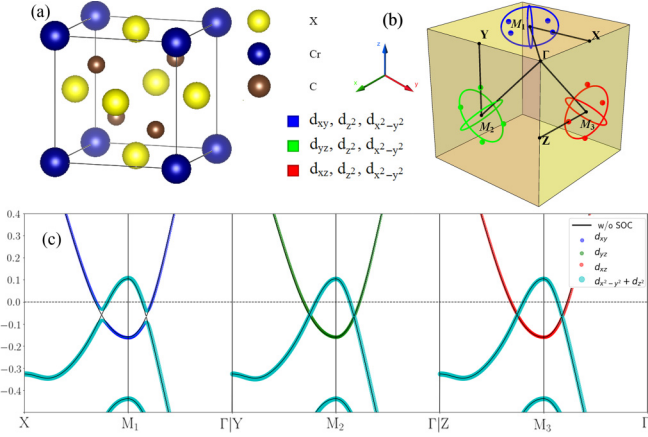


FIG. 2. The lattice structure and electronic structure of C_4CrX_3 . (a) The lattice structure of C_4CrX_3 . (b) Weyl points of C_4CrSi_3 in a reciprocal lattice without SOC: The color lines show the main contribution of partial density of states near the gapless points in the first Brillouin zone, and the solid lines show the high symmetry path in (c). (c) Band structure (without SOC) and fat band structure (with SOC, magnetization direction along 001 directions) of C_4CrSi_3 . The k path is shown in (b) where without considering SOC there are no gapless points along high symmetry lines, and the gap is open in X - M_1 - Y . The colors show four different orbit contributions.

$\theta = \frac{\pi}{2}$. However, as discussed above, when the mirror operation is a linear combination of σ_x and σ_y , we have to consider the combination of TRS and mirror symmetry. Taking the TRS operator T as $i\sigma_y K \otimes I$ with K indicating the complex conjugate, we have also $[H, MT] = 0$, $[H, P_C T] = 0$, if and only if $\theta = \frac{\pi}{2}$. That is, for $\theta = \frac{\pi}{2}$, regardless of the resulting spin matrix in the presence of SOC, the original symmetry of the Hamiltonian $H_{ij}(\mathbf{k})$ will not be further lowered, i.e., the topological nodal-line state is untouched. On the other hand, when $\theta \neq \frac{\pi}{2}$, the SOC will break the combination of TRS and mirror/ C_2 symmetries, leading to the reduction of the nodal line into Weyl points. In this sense, the topological properties are protected by a combination of TRS and mirror/ C_2 rotation symmetries, and tuning the magnetization direction can effectively change the topological nature of the electronic states. This is consistent with our observation of the three-band lattice model [Eq. (3)], where nodal lines are protected by the mirror/ C_2 symmetries without SOC, but will be reduced to Weyl nodes after considering SOC if $\theta \neq \frac{\pi}{2}$, i.e., if the magnetization is not in the $\theta \neq \frac{\pi}{2}$ plane.

Turning now to the realization of such a lattice model which is in principle applicable to all materials with the point group D_{2d} , we propose that magnetization-direction tunable topological states can be achieved in C_4CrX_3 ($X = \text{Ge}$ and Si). It is noted that both C_4CrSi_3 and C_4CrGe_3 are predicted to host the spin gapless semiconducting state [43,44].

For C_4CrX_3 , the crystal structure is shown in Fig. 2. The crystalline space group is $P\bar{4}3m$, leading to the T_d point group symmetry. There are six mirror reflection planes, namely, (011), (01 $\bar{1}$), (101), (10 $\bar{1}$), (110), (11 $\bar{0}$) planes, and the three C_2 rotation axes are the x , y , z axes, respectively. To identify the gapless points in the Brillouin zone with and without SOC, non-self-consistent DFT calculations are performed on a very

TABLE I. Weyl points and nodal-line dependence on the magnetization direction.

Magnetization direction	WPs (pairs)	Nodal line
Without SOC	6	6
001	8	4
010	8	4
100	8	4
011	10	2
101	10	2
110	10	2
111	12	0

dense \mathbf{k} mesh. For the case without SOC, we find six pairs of Weyl points and six nodal lines lying exactly on the six mirror planes. It is noted that the Weyl points and nodal lines can be divided into three sets, each containing four Weyl points and two nodal lines (Fig. 2). It is observed that each set of Weyl points and nodal lines can be attributed to different d orbitals, based on the fat band plots, as shown in Fig. 2(c). For instance, for M_1 (0.5, 0.5, 0), the relevant orbitals are the $\{d_{xy}, d_{z^2}, d_{x^2-y^2}\}$ orbitals, while for M_2 (0, 0.5, 0.5) and M_3 (0.5, 0, 0.5), the orbitals originate from the $\{d_{yz}, d_{z^2}, d_{x^2-y^2}\}$ orbitals and the $\{d_{xz}, d_{z^2}, d_{x^2-y^2}\}$ orbitals, respectively. Focusing on the $\{d_{xy}, d_{z^2}, d_{x^2-y^2}\}$ orbitals at M_1 (0.5, 0.5, 0), it is observed that without SOC, there exist two nodal lines lying on the M_{110} and $M_{\bar{1}10}$ mirror planes, and two pairs of Weyl nodes on the C_{2x} and C_{2y} rotation axes. This corresponds to the black lines in the left panel of Fig. 2(c). After considering SOC with the magnetization direction along (001), the degeneracy in the nodal lines is lifted, resulting in two more pairs of Weyl nodes. Correspondingly, a finite band gap is opened, as shown in the left panel of Fig. 2(c). This is consistent with our analysis using the lattice model in previous discussions. At M_1 (0.5, 0.5, 0), the corresponding isotropy group is D_{2d} , with the resulting bands from the $\{d_{xy}, d_{z^2}, d_{x^2-y^2}\}$ orbitals behaving exactly the same as expected based on the lattice model.

The symmetry arguments can be further applied to understand the band structure at other M points. It is noted that d_{xy} , d_{yz} , and d_{xz} form the basis of the three-dimensional irreducible representation of the T_d point group. Therefore, without SOC, the bands at M_1 , M_2 , and M_3 are related to each other by the C_3 rotation along the [111] axis, where the band character changes depending on the M points [Fig. 2(c)]. After considering SOC, as shown in Fig. 2(c) for $\mathbf{M} \parallel (001)$, the band gap is only opened between bands from the $\{d_{xy}, d_{z^2}, d_{x^2-y^2}\}$ orbitals at M_1 , while for the bands from the $\{d_{yz}, d_{z^2}, d_{x^2-y^2}\}$ orbitals at M_2 and the $\{d_{xz}, d_{z^2}, d_{x^2-y^2}\}$ orbitals at M_3 the degeneracy is kept. Such degeneracies for bands from the $\{d_{yz}, d_{z^2}, d_{x^2-y^2}\}$ and $\{d_{xz}, d_{z^2}, d_{x^2-y^2}\}$ orbitals lead to nodal lines on the (011) and (101) planes, respectively. Based on the lattice model presented in previous discussions, such nodal lines are protected by the fact that the magnetization direction is perpendicular to the mirror planes such as (011) and (101), i.e., $\theta = \frac{\pi}{2}$ effectively.

In Table I, the number of Weyl points and nodal lines from DFT calculations are shown for cases without SOC and

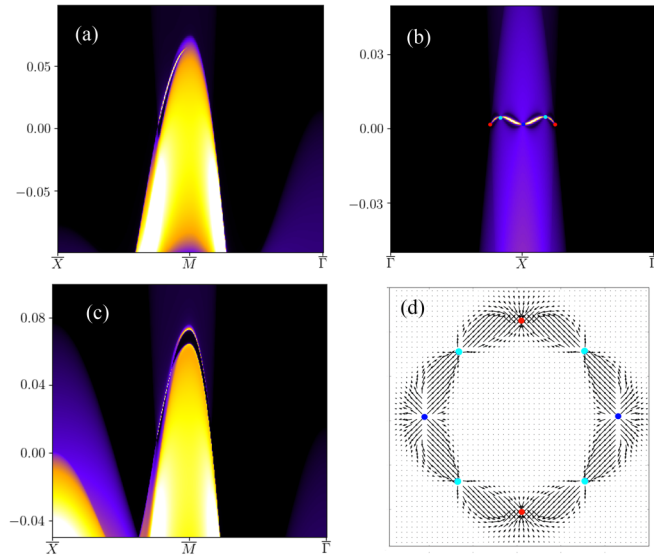


FIG. 3. Surface states and Berry curvature. (a) Surface electronic structure projected onto the (001) surface. (b) Surface electronic structure projected onto the (010) surface. (c) Surface states on the (001) plane obtained with $\xi = 0.04$, $\theta = \frac{\pi}{4}$. (d) The distribution of Berry curvature in the red square highlighted in (c), where the arrows indicate the x, y component of the Berry curvature, the blue (red) solid circles denote Weyl nodes with chirality +1 (-1), and the cyan solid circles correspond to (b) the gapless points of the nodal lines in the (001) plane.

with SOC for several magnetization directions. That is, after considering SOC, the number of pairs of Weyl points n_{wp} and nodal lines n_{nl} satisfy $n_{\text{wp}} + n_{\text{nl}} = 12$. Such a conservation law is guaranteed by the symmetry, e.g., each pair of perpendicular mirror planes define an axis, and two nodal lines will be protected when the magnetization direction is perpendicular to the axis, corresponding to the $\theta = \pi/2$ case as discussed above. Therefore, the resulting number of nodal lines n_{nl} is always two times the number of axes (k_x, k_y, k_z) which are perpendicular to the magnetization direction.

The topological nature of the electronic structure can be explicitly visualized from the surface states. Figure 3 shows the surface states and the distribution of the Berry curvature for $\theta = \frac{\pi}{2}$ of the three-band D_{2d} lattice model. Without any loss of physics, here we set the $H_{\perp} = 0$, i.e., we consider a spinless model as given by Eq. (3). It is noted that the surface states shown in Fig. 3 are in good agreement with those obtained based on DFT calculations (cf. Supplemental Material [40]).

Obviously, in the case without SOC, there are Fermi arcs connecting two Weyl nodes. As shown in Fig. 3(a), on the (001) surface, the Fermi arcs connect the Weyl nodes from

the blue group [Fig. 2(b)]. Actually, due to the presence of the nodal lines, the Fermi arcs from \bar{X} to \bar{M} merge into the projected drumhead surface states originating from the nodal lines. The chirality of the Weyl nodes is clearly evidenced by the distribution of the Berry curvature [Fig. 3(d)], where the Berry curvature “flows out” of the Weyl points with chirality +1 (blue points), “passes by” the points of the nodal line (cyan points), and finally “flows into” the Weyl points with chirality -1 (red points). On the (010) surfaces [Fig. 3(b)], two Weyl points are projected onto the \bar{X} points, and the other two Weyl points are located on each side of \bar{X} on the line Γ - \bar{X} . Additionally, there are two gapless points from the projected nodal lines. After considering SOC, when $\theta = \frac{\pi}{2}$, the derived surface states (not shown) are exactly the same with the corresponding cases without SOC [Figs. 3(a) and 3(b)]. However, when $\theta \neq \frac{\pi}{2}$, the SOC breaks the combination of mirror and time-reversal symmetry following the analysis in previous discussions, leading to a reduction of nodal lines into Weyl points. In Fig. 3(c), it is clear that at \bar{M} the degeneracy in the nodal lines has been lifted, resulting in a local band gap. In this case, on the projected surface states, the original Weyl points are no longer connected to the nodal lines, and the Fermi arcs lie between two Weyl points along the \bar{X} - \bar{M} section. After further investigation, it is noticed that four of the eight Weyl points are type-II Weyl points.

To summarize, we have developed a three-band lattice tight-binding model for the D_{2d} point groups for the d_{z^2} , d_{xy} , and $d_{x^2-y^2}$ orbitals, where nodal lines and Weyl points coexist. It is observed that the magnetization direction can be used to tailor the electronic structure and hence the topological properties. A detailed symmetry analysis reveals that a combination of mirror and time-reversal symmetry can protect the occurrence of nodal lines for specific magnetization directions even after considering SOC. In addition, we put forward a different class of materials C_4CrX_3 ($X = \text{Ge}$ and Si) where the three-band model can be applied and demonstrated explicitly that the number of nodal lines and Weyl points depends on the magnetization direction. We suspect that in other real materials with the essential symmetry, such a magnetization-direction tunable topological phase transition should exist, awaiting further theoretical and experimental explorations.

We thank Gui-Bin Liu for insightful discussions. The work is supported by the National Key R&D Program of China (Grant No. 2016YFA0300600), the NSF of China (Grants No. 11734003, No. 11574029, and No. 11774028), and also the Basic Research Funds of Beijing Institute of Technology (No. 2017CX01018). H.Z. acknowledges the financial support of the DFG-SPP 1666 program, and both Z.Z. and Q.G. are supported by the CSC scholarship. The calculations were performed on the Lichtenberg supercomputer.

- [1] H. B. Nielsen and M. Ninomiya, *Phys. Lett. B* **130**, 389 (1983).
- [2] A. A. Burkov, M. D. Hook, and L. Balents, *Phys. Rev. B* **84**, 235126 (2011).
- [3] A. A. Burkov and L. Balents, *Phys. Rev. Lett.* **107**, 127205 (2011).

- [4] X. Wan, A. M. Turner, A. Vishwanath, and S. Y. Savrasov, *Phys. Rev. B* **83**, 205101 (2011).
- [5] T. Bzdušek, Q. Wu, A. Rüegg, M. Sigrist, and A. A. Soluyanov, *Nature (London)* **538**, 75 (2016).
- [6] H. Weng, C. Fang, Z. Fang, B. A. Bernevig, and X. Dai, *Phys. Rev. X* **5**, 011029 (2015).

- [7] M. Ezawa, *Phys. Rev. Lett.* **116**, 127202 (2016).
- [8] C. Fang, H. Weng, X. Dai, and Z. Fang, *Chin. Phys. B* **25**, 117106 (2016).
- [9] R. Yu, Q. Wu, Z. Fang, and H. Weng, *Phys. Rev. Lett.* **119**, 036401 (2017).
- [10] M. Hirayama, R. Okugawa, T. Miyake, and S. Murakami, *Nat. Commun.* **8**, 14022 (2017).
- [11] J. Ruan, S.-K. Jian, H. Yao, H. Zhang, S.-C. Zhang, and D. Xing, *Nat. Commun.* **7**, 11136 (2016).
- [12] A. A. Soluyanov, D. Gresch, Z. Wang, Q. Wu, M. Troyer, X. Dai, and B. A. Bernevig, *Nature (London)* **527**, 495 (2015).
- [13] Z. Yan, R. Bi, H. Shen, L. Lu, S.-C. Zhang, and Z. Wang, *Phys. Rev. B* **96**, 041103(R) (2017).
- [14] H. Weng, Y. Liang, Q. Xu, R. Yu, Z. Fang, X. Dai, and Y. Kawazoe, *Phys. Rev. B* **92**, 045108 (2015).
- [15] L. X. Yang, Z. K. Liu, Y. Sun, H. Peng, H. F. Yang, T. Zhang, B. Zhou, Y. Zhang, Y. F. Guo, M. Rahn, D. Prabhakaran, Z. Hussain, S.-K. Mo, C. Felser, B. Yan, and Y. L. Chen, *Nat. Phys.* **11**, 728 (2015).
- [16] B. Q. Lv, N. Xu, H. M. Weng, J. Z. Ma, P. Richard, X. C. Huang, L. X. Zhao, G. F. Chen, C. E. Matt, F. Bisti, V. N. Strocov, J. Mesot, Z. Fang, X. Dai, T. Qian, M. Shi, and H. Ding, *Nat. Phys.* **11**, 724 (2015).
- [17] S.-Y. Xu, I. Belopolski, N. Alidoust, M. Neupane, G. Bian, C. Zhang, R. Sankar, G. Chang, Z. Yuan, C.-C. Lee, S.-M. Huang, H. Zheng, J. Ma, D. S. Sanchez, B. Wang, A. Bansil, F. Chou, P. P. Shibayev, H. Lin, S. Jia, and M. Z. Hasan, *Science* **349**, 613 (2015).
- [18] B. Q. Lv, H. M. Weng, B. B. Fu, X. P. Wang, H. Miao, J. Ma, P. Richard, X. C. Huang, L. X. Zhao, G. F. Chen, Z. Fang, X. Dai, T. Qian, and H. Ding, *Phys. Rev. X* **5**, 031013 (2015).
- [19] G. Bian, T.-R. Chang, R. Sankar, S.-Y. Xu, H. Zheng, T. Neupert, C.-K. Chiu, S.-M. Huang, G. Chang, I. Belopolski, D. S. Sanchez, M. Neupane, N. Alidoust, C. Liu, B. Wang, C.-C. Lee, H.-T. Jeng, C. Zhang, Z. Yuan, S. Jia *et al.*, *Nat. Commun.* **7**, 10556 (2016).
- [20] M. Hirschberger, S. Kushwaha, Z. Wang, Q. Gibson, S. Liang, C. Belvin, B. Bernevig, R. Cava, and N. Ong, *Nat. Mater.* **15**, 1161 (2016).
- [21] X. Chen, Z.-C. Gu, Z.-X. Liu, and X.-G. Wen, *Phys. Rev. B* **87**, 155114 (2013).
- [22] Y.-H. Chan, C.-K. Chiu, M. Y. Chou, and A. P. Schnyder, *Phys. Rev. B* **93**, 205132 (2016).
- [23] G. Bian, T.-R. Chang, H. Zheng, S. Velury, S.-Y. Xu, T. Neupert, C.-K. Chiu, D. S. Sanchez, I. Belopolski, N. Alidoust, P.-J. Chen, G. Chang, A. Bansil, H.-T. Jeng, H. Lin, and M. Z. Hasan, *Phys. Rev. B* **93**, 121113(R) (2016).
- [24] B. Z. Spivak and A. V. Andreev, *Phys. Rev. B* **93**, 085107 (2016).
- [25] A. Cortijo, D. Kharzeev, K. Landsteiner, and M. A. H. Vozmediano, *Phys. Rev. B* **94**, 241405 (2016).
- [26] E. Khalaf and P. M. Ostrovsky, *Phys. Rev. Lett.* **119**, 106601 (2017).
- [27] Z. Long, Y. Wang, M. Erukhimova, M. Tokman, and A. Belyanin, *Phys. Rev. Lett.* **120**, 037403 (2018).
- [28] C. Shekhar, A. K. Nayak, S. Singh, N. Kumar, S.-C. Wu, Y. Zhang, A. C. Komarek, E. Kampert, Y. Skourski, J. Wosnitza, W. Schnelle, A. McCollam, U. Zeitler, J. Kubler, S. S. P. Parkin, B. Yan, and C. Felser, [arXiv:1604.01641](https://arxiv.org/abs/1604.01641).
- [29] S. Borisenko, D. Evtushinsky, Q. Gibson, A. Yaresko, T. Kim, M. N. Ali, B. Buechner, M. Hoesch, and R. J. Cava, [arXiv:1507.04847](https://arxiv.org/abs/1507.04847).
- [30] Y. J. Jin, R. Wang, Z. J. Chen, J. Z. Zhao, Y. J. Zhao, and H. Xu, *Phys. Rev. B* **96**, 201102(R) (2017).
- [31] Z. Wang, M. Vergniory, S. Kushwaha, M. Hirschberger, E. V. Chulkov, A. Ernst, N. P. Ong, R. J. Cava, and B. A. Bernevig, *Phys. Rev. Lett.* **117**, 236401 (2016).
- [32] R. Wang, Y. J. Jin, J. Z. Zhao, Z. J. Chen, Y. J. Zhao, and H. Xu, *Phys. Rev. B* **97**, 195157 (2018).
- [33] H. Yang, Y. Sun, Y. Zhang, W.-J. Shi, S. S. P. Parkin, and B. Yan, *New J. Phys.* **19**, 015008 (2017).
- [34] L. Smejkal, J. Zelezny, J. Sinova, and T. Jungwirth, *Phys. Rev. Lett.* **118**, 106402 (2017).
- [35] K. Kuroda, T. Tomita, M.-T. Suzuki, C. Bareille, A. Nugroho, P. Goswami, M. Ochi, M. Ikhlas, M. Nakayama, S. Akebi, R. Noguchi, R. Ishii, N. Inami, K. Ono, H. Kumigashira, A. Varykhalov, T. Muro, T. Koretsune, R. Arita, S. Shin, T. Kondo, and S. Nakatsuji, *Nat. Mater.* **16**, 1090 (2017).
- [36] X. Huang, L. Zhao, Y. Long, P. Wang, D. Chen, Z. Yang, H. Liang, M. Xue, H. Weng, Z. Fang, X. Dai, and G. Chen, *Phys. Rev. X* **5**, 031023 (2015).
- [37] D. MacNeill, G. M. Stiehl, M. H. D. Guimaraes, R. A. Buhrman, J. Park, and D. C. Ralph, *Nat. Phys.* **13**, 300 (2016).
- [38] J.-P. Hanke, F. Freimuth, C. Niu, S. Blügel, and Y. Mokrousov, *Nat. Commun.* **8**, 1479 (2017).
- [39] G.-B. Liu, W.-Y. Shan, Y. Yao, W. Yao, and D. Xiao, *Phys. Rev. B* **88**, 085433 (2013).
- [40] See Supplemental Material at <http://link.aps.org/supplemental/10.1103/PhysRevB.98.121103> for computational details, which includes Refs. [45–49].
- [41] C. Niu, P. M. Buh, H. Zhang, G. Bihlmayer, D. Wortmann, S. Blügel, and Y. Mokrousov, [arXiv:1703.05540](https://arxiv.org/abs/1703.05540).
- [42] H. Takayama, K.-P. Bohnen, and P. Fulde, *Phys. Rev. B* **14**, 2287 (1976).
- [43] M. Rostami, M. Moradi, Z. Javdani, and H. Salehi, *Mater. Sci. Semicond. Process.* **38**, 218 (2015).
- [44] Y.-S. Kim and Y.-C. Chung, *IEEE Trans. Magn.* **41**, 2733 (2005).
- [45] G. Kresse and J. Hafner, *Phys. Rev. B* **47**, 558 (1993).
- [46] G. Kresse and J. Furthmüller, *Phys. Rev. B* **54**, 11169 (1996).
- [47] J. P. Perdew, K. Burke, and M. Ernzerhof, *Phys. Rev. Lett.* **77**, 3865 (1996).
- [48] M. P. L. Sancho, J. M. L. Sancho, J. M. L. Sancho, and J. Rubio, *J. Phys. F: Met. Phys.* **15**, 851 (1985).
- [49] A. A. Mostofi, J. R. Yates, G. Pizzi, Y.-S. Lee, I. Souza, D. Vanderbilt, and N. Marzari, *Comput. Phys. Commun.* **185**, 2309 (2014).